Fermi National Accelerator Laboratory

FN-398
1620.000
(Submitted to
Nucl. Instrum. Methods)

SYMMETRIC AND NON-SYMMETRIC LAMBERTSON MAGNETS

M. Harrison and F. N. Rad

February 1984

Operated by Universities Research Association Inc. under contract with the United States Department of Energy

Symmetric and Non-Symmetric Lambertson Magnets

M. Harrison and F.N. Rad

Fermi National Accelerator Laboratory Batavia, Illinois 60510

Received February 24, 1984

A set of symmetric and non-symmetric Lambertson magnets has been designed for the injection, extraction, and abort line of Fermi National Accelerator Laboratory superconducting synchrotron. Techniques, measurements, and detailed analysis of both body and end field are presented.

1. Introduction

Beam splitting requirements of the Fermi National Accelerator Laboratory superconducting synchrotron necessitated the design of different high field (--9, 11, and 15 kilogauss) symmetric and non-symmetric Lambertson magnetic septa. These Lambertson magnets were designed to minimize the remnant field in the field-free-region and were built for use in the injection, abort, and extraction lines. In addition, special end skirts were implemented to reduce flux leakage from the dipole region making a large contribution to the integral field of the field-free-region.

2. Experimental Setup

Magnet stands employed in the field measurements were two separate tables with X and Y lathes. The stands were anchored to the floor, leveled and parallel to each other, and positioned several feet from the ends of the magnet.

Power supplies utilized for all the measurements were a quarter megawatts Transrex 240-12, and a half megawatts Transrex 500-5. Power supply stability over long time intervals is within a few ampere range. An external Leeds & Northrup current shunt with 0.1% accuracy was employed for measuring magnet current. In conjunction with the shunt a Dana 5900 digital volt meter was used. Ripples measured at the field coil is approximately 0.2%.

A single wire loop (Cu-Be alloy), extending several feet beyond the ends of the total magnet, separated by 0.250 inches was employed for integral field measurements for both dipole-field and field-free regions. If V and T are defined to be the induced voltage on the single wire loop and the integrator time constant, then the relationship for the integral field is simply

$$\int B \cdot dl = 4VT.$$

The stretched wire loop was held at both ends by mounts with capability of rotating into 90, 180, and 270 degree positions. This capability was highly desirable for measurements inside the field-free-region where X and Y components of the field were to be known for the non-symmetric Lambertson magnets.

In order to make accurate differential (dB/B) field measurements of the total dipole field, in conjunction with the stretched wire loop, a single wire loop extending half the length of the magnet over a square aluminum block of 0.50 inch in thickness (twice the width of the stretched wire) was used. This single wire loop referred to as dummy coil was positioned at a fixed region of the dipole field. Using the above relationship for the stretched wire loop and the dummy coil, the relationship for dB/B at position j with respect to position i, to the first order, is simply

$$dB_j/B_j = (dV_i - dV_j)/V_j,$$

where dV_i is the difference in the induced voltage in wire loop and dummy coil at position i, and dV_j is the difference in the induced voltage in wire loop and dummy coil at position j. V_j is the induced voltage on the stretched wire loop at position j.

The use of this dummy coil minimizes large jitter in the induced voltage at peak current and was positioned so the difference in the induced voltage on the wire loop and the dummy coil was a small positive number. Differential field measurements were then obtained by scanning the dipole-field-region with the stretched wire loop.

The excitation curves and body field were measured with a small multiturn point coil mounted on a G-10 plate, and the fringe-field-region of the magnets were sampled with a Hall probe. All field measurements, with the exception of Hall probe, were done with the power supply at ramped mode, and recorded before the start of the ramp and at the flat top of the ramp (magnet at full power). This technique allows correction for residual field for each cycle. In addition, in order to reduce uncertainties in local variations, multiple measurements were made at each position.

3. Design Consideration

The end profile of the symmetric and non-symmetric Lambertson magnets, designed and implemented in Fermilab's superconducting synchrotron are shown in figure 1. The dipole-field and field-free-regions are clearly seen. For measurements and presentation of the results a set of coordinate systems for each magnet was chosen. The X and Y axes of these coordinate systems for each magnet are clearly shown. The Z-axis is defined to be along the particle trajectory beginning at the pole face edge.

As particles pass through the magnet they experience an integral field inside the magnet. In Lambertson magnets this integral field in the dipole-field-region is an order of magnitude larger than the integral field in the field-free-region. Therefore due to the presence of a large dipole-fringe-field, the field in front of the entrance and exit windows of the field-free-region are much larger than the field inside the field-free-region. Thus these fringe fields can increase the integral field seen by the particles passing through the field-free-region by several factors.

One of the important criteria in the design of a Lambertson magnet is the minimization of fringe field leakage from dipole-field-region into the field-free-region at the ends of the magnet. To accomplish this, one technique is to shorten one pole with respect to the pole containing the field free hole. Although this technique will reduce the strength of the fringe field, it will also distort the field gradient inside the dipole field as shown in figure 2. This figure shows dB/B versus Y for the non-symmetric injection Lambertson magnet shown in figure 1b across the transition region, where the recessed pole face lies, in steps of 2.54 mm. As seen there is a large rate of change of field in this region.

To further reduce the fringe field, in addition to the above technique, another technique can be implimented. This involves placing of skirts* at the ends of the magnet at an appropriate distance from the pole face. Several tests with an iron plate of 0.5 inches in thickness showed that a separation of 0.5 inches between the magnet-pole-face and the skirt will result in minimum fringe field in the region of the field-free-region. However in order to determine both size and thickness of the end skirts, the magnetic field at a fixed point in the region of the field-free-region was measured as a function of the number of lamination for two different size lamination plates. These results are shown in figure 3. Curve a shows the results of our measurements using the same size lamination as was used in the magnet. A second set of 16x16 square inch non-symmetric lamination plates were made in order to cover the entire face of the magnet, especially the magnet coils. The results of our measurements are shown by curve b, giving the ideal results. The overall effect of this end skirt on the fringe field in the field-free-region is clearly seen in figure 4. The dramatic decrease in the fringe field in the region of the

field-free-region, shown by curve b, as compared with the measurements without end skirt, depicted by curve a, is clearly seen.

Based on these measurements special end skirts equal in thickness to ten laminations (9.5 mm) were designed and implemented.

4. Poisson Calculation

All field calculations associated with the design of these Lambertson magnets were made using the Poisson group of programs running on a VAX 11/780. A typical magnet lattice consisted of approximately 10,000 mesh points with resolution varying between 0.05 inches in the septum region of the magnet up to 0.2 inches in the more homogenous areas of the steel. There was no strong correlation between mesh size and magnetic fields. The high resolution mesh in the septum area permitted a more accurate modelling of the physical geometry in this region. The B-H curves used by the programs were obtained from direct measurements on Republic Steel's Locore B which was used in the magnet construction. A generic low carbon B-H produced essentially identical results indicating that the magnetic properties were not critically dependent upon steel saturation. A typical magnet simulation run used four to five hours of CPU time, less than ten such runs resulted in a final magnet design.

5. Results

Results of our measurements for the symmetric and non-symmetric Lambertson magnets along with Poisson calculations are presented below for all three magnets. The symmetric Lambertson magnet, an end profile of which is shown in figure 1a, was designed for use in the abort and up-stream end of the extraction lines. The results of our measurements for this magnet are given in detail in subsection 5.1.

Two sets of non-symmetric Lambertson magnets were designed and implemented. The first set, an end profile of which is shown in figure 1b, is primarily for use in the injection lines for both proton and anti-proton beam and will be described in subsection 5.2. The highly non-symmetric Lambertson magnet shown in figure 1c was primarily used in the down-stream end of the extraction line. The results of these magnets will be given in subsection 5.3.

As indicated above, all integral measurements were made with a single stretched wire loop. The differential measurements were made with a dummy coil in conjunction with the stretched wire. Body field and fringe field measurements were done with a small multiturn point coil along with a Hall probe.

In order to determine the accuracy of our measurements, background, and the integrator drift, each point was repeated several times.

5.1. Symmetric Lambertson Magnets:

The end profile of this magnet is shown in figure 1a. Also for clarity, the X and Y coordinate system used in all the measurements is clearly indicated in the figure.

The X component of the integral field, $\int Bx.dl$ in the field-free-region, is shown by curve a of figure 5. Although not shown, $\int By.dl$ for this magnet was measured and was a constant value (9+-2 gauss-meter) across the field-free-region. Curve C shows the $\int Bx.dl$ with end skirts which is in good qualitative agreement with Poisson calculation shown as curve b. The observed differences between curves b and c are due to the use of thinner end skirts than was needed for this magnet. As shown by curve d the effects of trim coils in the field-free-region for this magnet appears to be negligible.

Similar measurements, as depicted in figure 4, had been performed for this magnet with similar effects when end-skirts were used to eliminate residual field caused by the dipole-field-region.

Figure 6 shows the differential field, dB/B versus Y in the dipole-field-region, for the symmetric Lambertson magnet. Curve a is the result of the overall field measurements without end skirts, and Curve b with end-skirts. Curves c and d are the results of body measurements and Poisson calculations, respectively. Poisson calculation is in disagreement with the measurements and there is no clear explanation of this discrepancy.

Figure 7 shows the $\int B.dl/I$ versus I for both field-free-region, depicted by curve a, and dipole-field-region, depicted by curve b. As seen there is a large flat region and the saturation begins shortly before maximum operating current of 4400 ampere, which does not appear to be true for non-symmetric Lambertson magnets (subsection 5.2, and 5.3).

5.2. Non-Symmetric Lambertson Magnets:

The end profile of this magnet is shown in figure 1b. The X, and Y coordinate system used in all measurements on this magnet are clearly seen.

The diferential field dB/B of the dipole-field-region was measured as a function of position Y at three different currents, 600, 1200, and 1800 ampere to an accuracy of +-1 x 10-4. These

measurements are shown by curves a, b, and c respectively in figure 8. Although quite similar in shape there is a large variation in the magnitude. At an operating current of 1575 ampere, similar measurement, is shown by curve a of figure 9. The effects of the end-skirts which are to reduce fringe-field effects and merge the overall integral-field to the integral body-field, are seen by curve b as being in good agreement with the body field measurements shown by curve c. However, Poisson calculations depicted by curve d is in gross disagreement with our body measurements.

The X and Y components of the integral field in the field-free-region are shown by curves a and b respectively in figure 10. The Y component of the field drops quite rapidly as one moves further away from the dipole field edge. The effect of the end-skirts are clearly seen by curve c which is in close agreement with the body-field measurements shown by curve d. Poisson calculations shown by X marks are in excellent agreement with the body field measurements.

In order to determine the saturation characteristics of this magnet, measurements were made beyond the operating current. Figure 11 shows the results of these measurements in the dipole-field-region. Curve a is from measurements away from the field-free hole, and shows a different saturation characteristic than the region in front of the field-free hole, as shown by shaded curve b. Poisson calculations are shown by X marks and do not reproduce the actual measurements. A similar measurement for the field-free-region is shown in figure 12. In this figure curves 1, 2, 3, and 4 are measurements at X positions of -1, -2, -3, and -4 centimeters from the dipole-field edge. Curve b is the result of body-field measurements at X = -2 Cm, and shaded curve p is the corresponding Poisson calculations at similar X positions of -1, -2, -3, and -4 centimeters. Once again there are large differences between body measurements and Poisson calculations.

5.3. Highly Non-Symmetric Lambertson

The end profile of this magnet is shown in figure 1c. The X and Y coordinate system used in all the measurements for this magnet is clearly indicated in this figure. This highly non-symmetric Lambertson magnet was designed for the down-stream end of the extraction line of Fermilab's superconducting synchrotron.

Because of the highly non-symmetric nature of this magnet, detail measurements of dipole-field and field-free regions were made. One such measurement is presented in figure 13. The integral field measurements were made along the expected particle trajectory at two different operating currents of 2217 ampere, shown by curve a, and the maximum operating current of 4435 ampere, shown by curve b. As seen there is a large variation of the field, experienced by the particles traversing the full length

of the magnet, across the dipole gap.

Figure 14 represents the saturation characteristics of the magnet across the field-free-region shown by curve b. Similar measurements for the body field in the dipole-field-region far away from the field-free hole is representd in figure 15.

A differential field measurement for the integrated field in the dipole-field-region is represented by curve a of figure 16. Similar measurements for the body is depicted by curve c. Poisson calculation is shown by curve b, which is in disagreement with the body measurements.

In the field-free-region, the integral field for the X and Y components of the field as a function of X position at Y = 0 are represented by curves a and b of figure 17, respectively. The X component of the integrated field shows a flat region between -2 and -5 centimeters, the region where particles are traversing. Although the Y component of the field shows an exponential drop off, it does show an average strength equal to that of the X component of the field in the region from -2 to -3 centimeters. Agreements between body-field measurements and Poisson calculations in the field-free-region, depicted by curves a and b of figure 18 respectively, are gratifying.

In the field-free-region, detailed matrix measurements of both the X-component of the integral field (as shown graphically in figure 19) and the Y-component of the integral field (difficult to show graphically) were made at two different currents of 3550 ampere and the full operating current of 4435 ampere, as a function of Y at four different X positions. These measurements at X positions of -1.5, -2.0 -2.5, -3.0 centimeters are shown in figure 20 by curves a, b, c, and d, respectively. Graphs I and II show our measurements at an operating current of 3550 ampere for the X and Y components of the integral field. Similarly graphs III and IV shows our measurements for X and Y components of the integral field at full operating current of 4435 ampere respectively. For comparison, Poisson calculations are shown by dashed curves and have been labled a' through d' to compare with curves a through d respectively.

There is a large disagreement, both in shape and magnitude, between the integral measurements, curves a through d, and Poisson calculations, curves a' through d'. Although difficult to design effective end-skirts for highly non-symmetric Lambertson magnet, it is our intuitive judgement that most of these differences, especially the differences in magnitude, would have been reduced had we incorporated end-skirts for this magnet.

6. Conclusion:

The magnets described above have been successfully implemented in the superconducting synchrotron facility at Fermi National Accelerator Laboratory.

Poisson calculations, as compared to all the results of our measurements for both symmetric and non-symmetric Lambertson magnets, reproduces body field inside the field-free-region with a great deal of success. On the other hand Poisson calculations have not been able to successfully reproduce body-field measurements in the dipole-field-region. This discrepancy could point toward possible narrowing of the dipole gap in the region of the field-free hole. This narrowing of the dipole field gap could have been caused by sagging due to lack of structural strength or non-symmetric welding of laminations on two sides of the magnets.

Based on the results of our measurements it is apparent that the end-skirts play an important role in not only shaping the fringe field but also reducing the integral field across the field-free-region. However, as was shown in figure 2, in the transition region there is a large differential field variation far greater than the expected magnet design specification. Perhaps this added complexity can be eliminated should one be able to reduce the fringe field by implementing end-skirts without having to recess one pole of the magnet. This will be studied in our next magnet design.

7. Acknowledgment

We are grateful to Mr. H.A. Koecher for his continuous support during the long arduous period of setting up the measuring facility and helping with the measurements. We wish to thank Miss Carmen Valdes for all the drawings in this paper.

* Also known by various other names such as; End-Plates, Field Catchers, and Fringe-Field-Quenchers.

8. Figure Captions:

Fig. 1, The end profile of Lambertson magnets. Diagram a--symmetric Lambertson magnet for abort and up-stream end of the extraction lines; Diagram b--non-symmetric Lambertson magnet used primarily in the injection lines; Diagram c--highly non-symmetric Lambertson magnet used in the down-stream end of the extraction line. The X and Y coordinates used for measurements are shown for each magnet. The Z coordinate, not shown, is taken into the paper along the particle trajectory.

Fig. 2, Differential field dB/B vs Y across the transition region in the dipole-field-region of the injection Lambertson. Curve a through k represent measurements beginning at Z = 10 Cm and in 2.54 mm increments respectively.

Fig. 3, The effect of lamination plates on the fringe field in front of the field-free-region of injection Lambertson. Curve a--results with same size lamination plates used in the actual magnet; Curve b--results of measurements with non-symmetric, 16x16 square inch, lamination plates.

Fig. 4, The effect of end skirts, similar to the ones used to produce curve b of figure 3 on the dipole-fringe-field in the region of the field-free-region as a function of Z. Curve a--results with no end-skirts; Curve b--results with 16x16 square inch non-symmetric end-skirts.

Fig. 5, The integral field $\int Bx.dl$ vs X in the field-free-region of the symmetric Lambertson. Curve a--integral measurements without end-skirts; Curve b--integral measurements with end skirts; Curve c--results of Poisson calculations; Curve d--integral field effects due to correction coils inside the magnet.

Fig. 6, Differential field dB/B vs Y in the dipole-field-region for the symmetric Lambertson magnet. Curve a--differential field measurements without end-skirts; Curve b--differential field measurements with end-skirts; Curve c--differential body field measurements; Curve d--results of Poisson calculation.

Fig. 7, Integral field $\int Bx.dl/I$ vs I for the symmetric Lambertson magnet. Curve a--measurements inside the field-free-region; Curve b--measurements inside the dipole-field-region.

Fig. 8, Differential field dB/B vs Y at X = 1Cm in the dipole-field-region; Curve a--results of measurements at 600 ampere; Curve b--results of measurements at 1200 ampere; Curve c--results of measurements at 1800 ampere.

Fig. 9, Differential field dB/B vs Y in the dipole-field-region at X = 1Cm at an operating current of 1575 ampere. Curve a--measurement without end skirt; Curve

b--measurement with end skirt; Curve c--results of body measurements; Curve d--results of Poisson calculation.

Fig. 10, Integral field 1B.dl vs X in the field-free-region at 1575 ampere. Curve a--1Bx.dl without end skirts; Curve c--same measurements with end skirts; Curve d--body measurements. The X marks are the results of Poisson calculations. Also for comparison, measurements of 1By.dl without end skirts are shown as curve b.

Fig. 11, 1B.dl/I vs I in the dipole-field-region at X = 1Cm; Curve a--measurements away from the hole at Y = 10Cm; Curve b--measurements in the region of the hole at Y = 0+-2 Cm. Poisson calculation results are indicated by an X mark.

Fig. 12, 1B.dl/I vs I in the field-free-region at y = 0; Curves 1, 2, 3, and 4 are measured at X = 1, 2, 3, and 4 Cm from the dipole field edge, respectively; Curve b--body measurement at X = -2 Cm; Curve p--results of Poisson calculation at x = 1, 2, 3, 4 Cm.

Fig. 13, Differential field dB/B vs X in the dipole-field-region for the highly non-symmetric Lambertson magnet along the expected particle trajectory. Curve a--results of the measurements at 2217 ampere; Curve b--results of the measurements at 4435 ampere.

Fig. 14, 1B.dl/I vs I for the highly non-symmetric Lambertson magnets. Curve a--measurements for the field-free-region; Curve b--measurements for the dipole-field-region.

Fig. 15, B/I vs I for the body field inside the dipole-field-region for the highly non-symmetric Lambertson magnets.

Fig. 16, Differential field dB/B vs Y in the dipole-field-region for the highly non-symmetric Lambertson magnet. Curve a--differential field measurements for the integrated field of the magnet; Curve C--differential body field measurements; Curve b--results of Poisson calculation.

Fig. 17, Integral field 1B.dl vs X in the field-free-region of the highly non-symmetric Lambertson magnet. Curve a--the X component of the integral field, 1Bx.dl; Curve b--the Y component of the integral field, 1By.dl.

Fig. 18, Body field versus X in the field-free-region of the highly non-symmetric Lambertson magnet. Curve a--results of the X component of the body field measurements; Curve b--Poisson calculation results.

Fig. 19, The X component of the integrated field as a function of X and Y in the field-free-region of the highly non-symmetric Lambertson magnet.

Fig. 20. The X and Y componet of the integrated field as a function of Y in the field-free-region of the highly non-symmetric Lambertson magnet. Curves a-d--resuts of measurements at X = -1.5, -2.0, -2.5, and -3.0 centimeters respectively; Curves a'-d'--Poisson calculation results at X = -1.5, -2.0, -2.5, and -3.0 centimeters respectively; Graphs I & II--results of the measurements at an operating current of 3550 ampere; Graphs III & IV--results of the measurements at maximum operating current of 4435 ampere.

Respectfully submitted,

Christian Rad

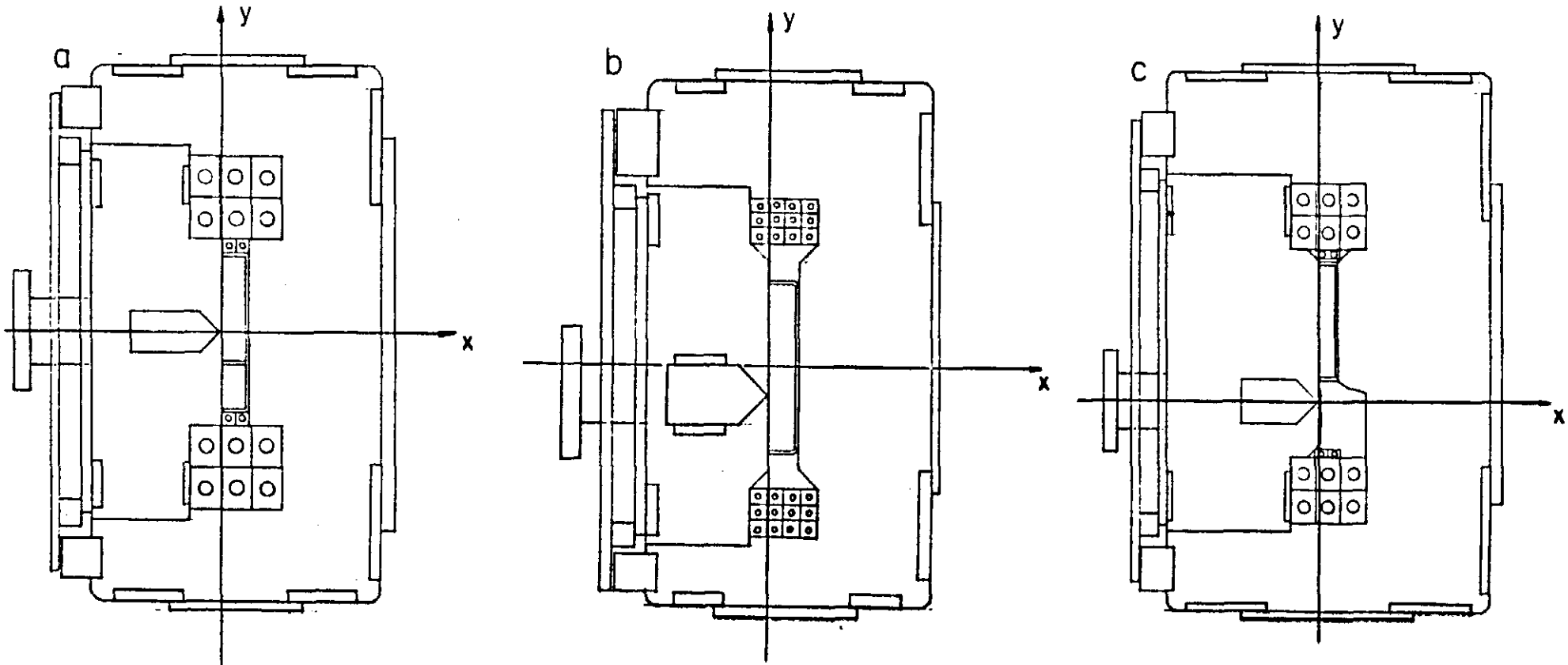

Figure 1

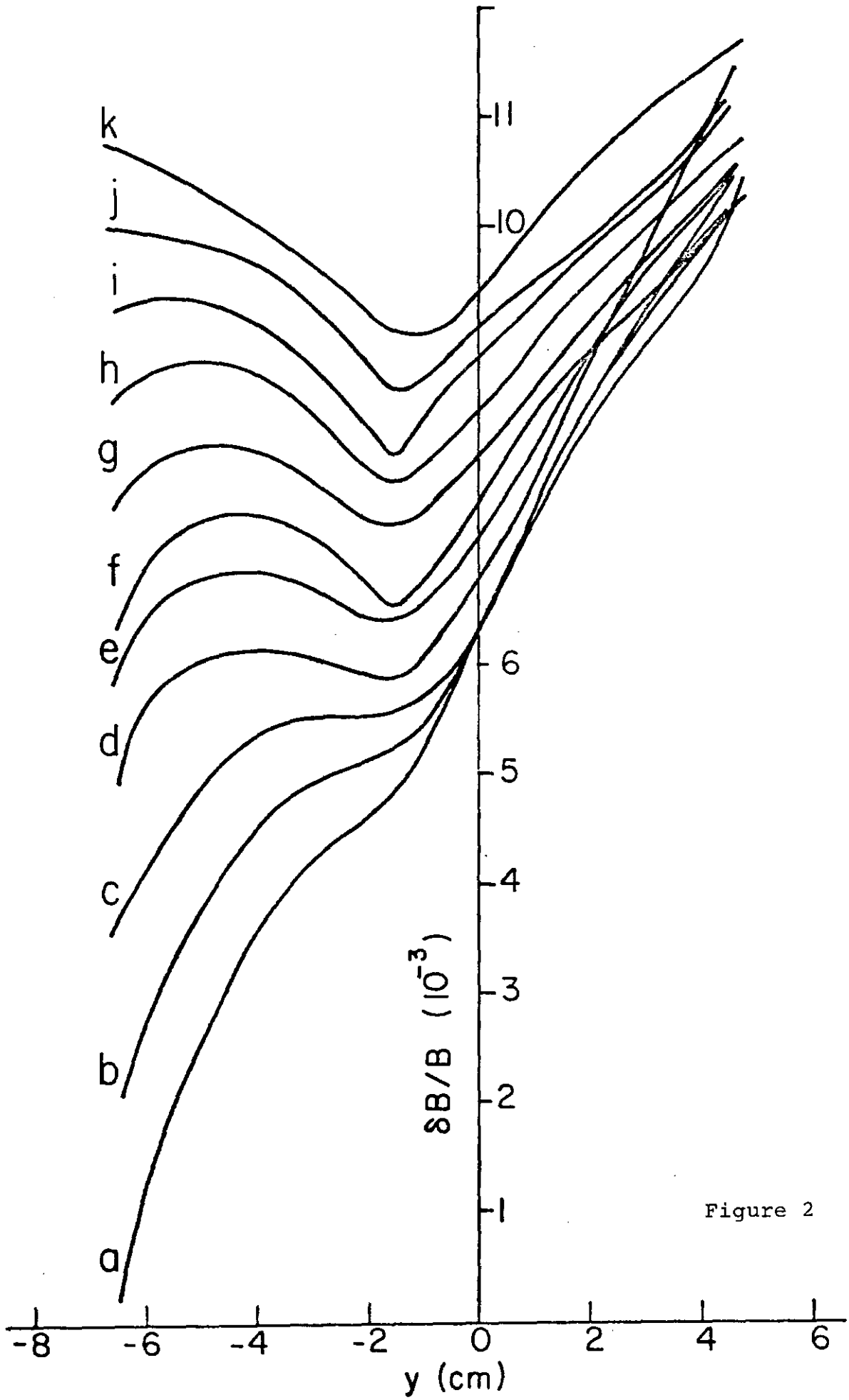

Figure 2

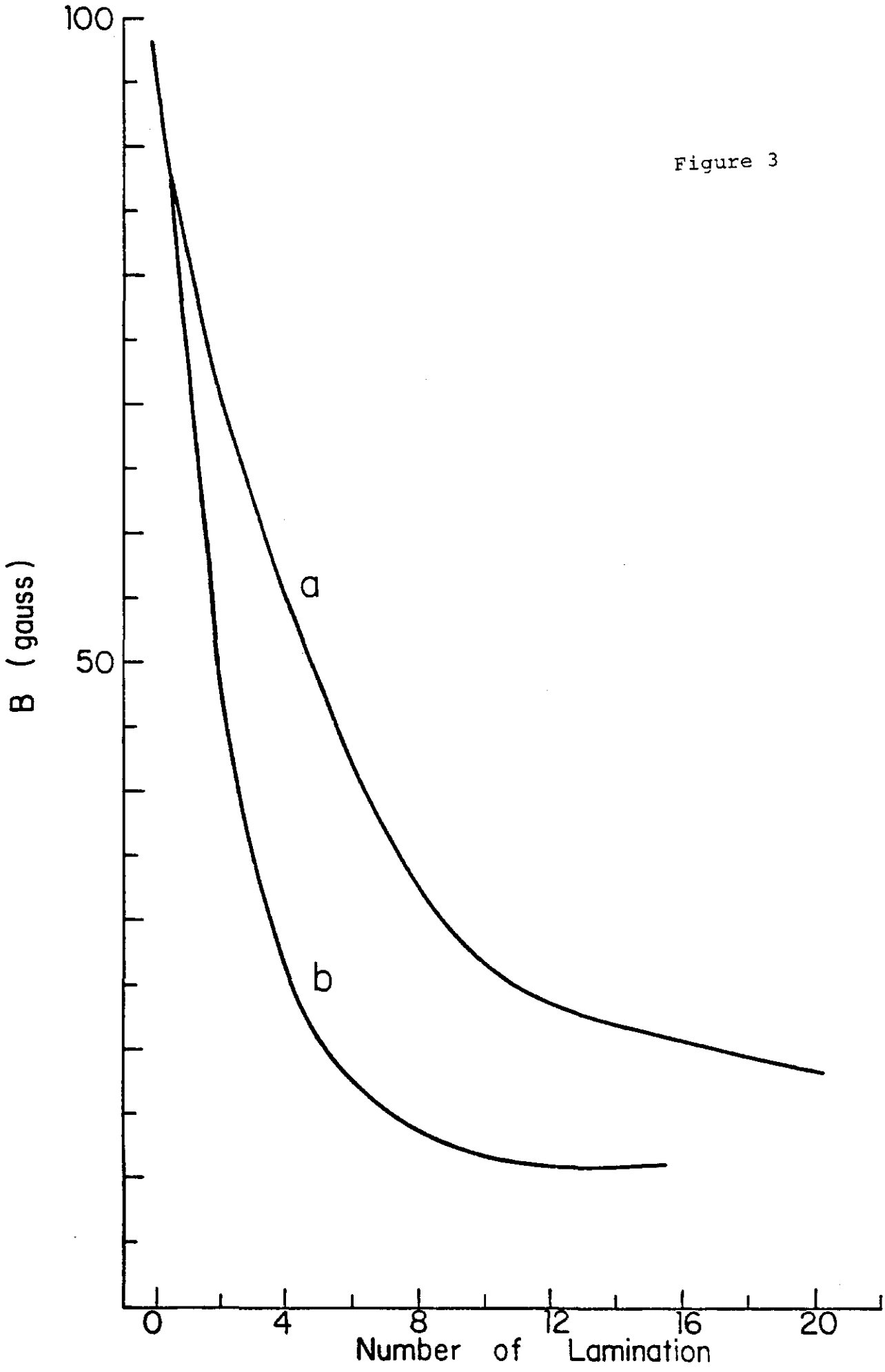

Figure 3

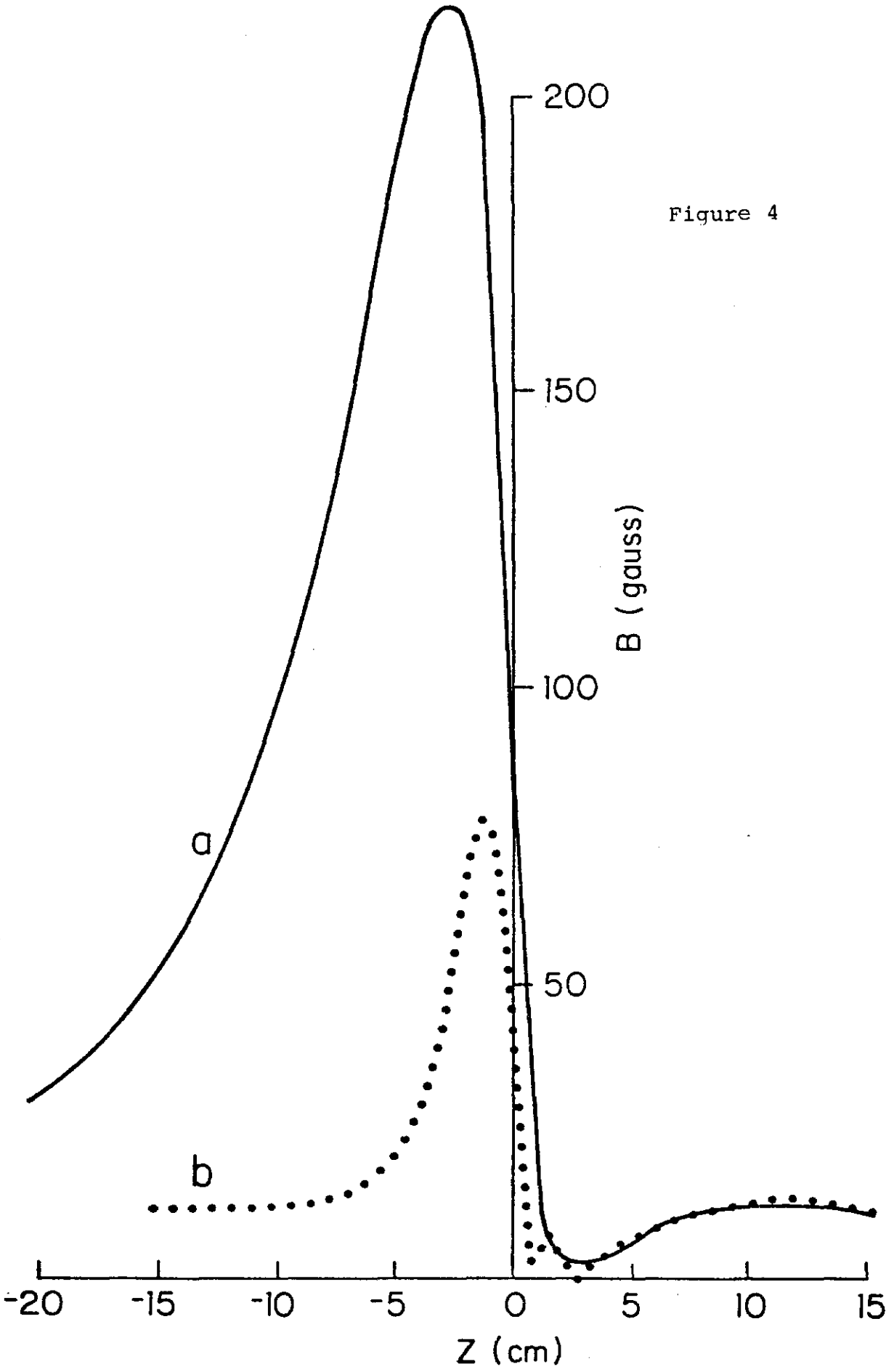

Figure 4

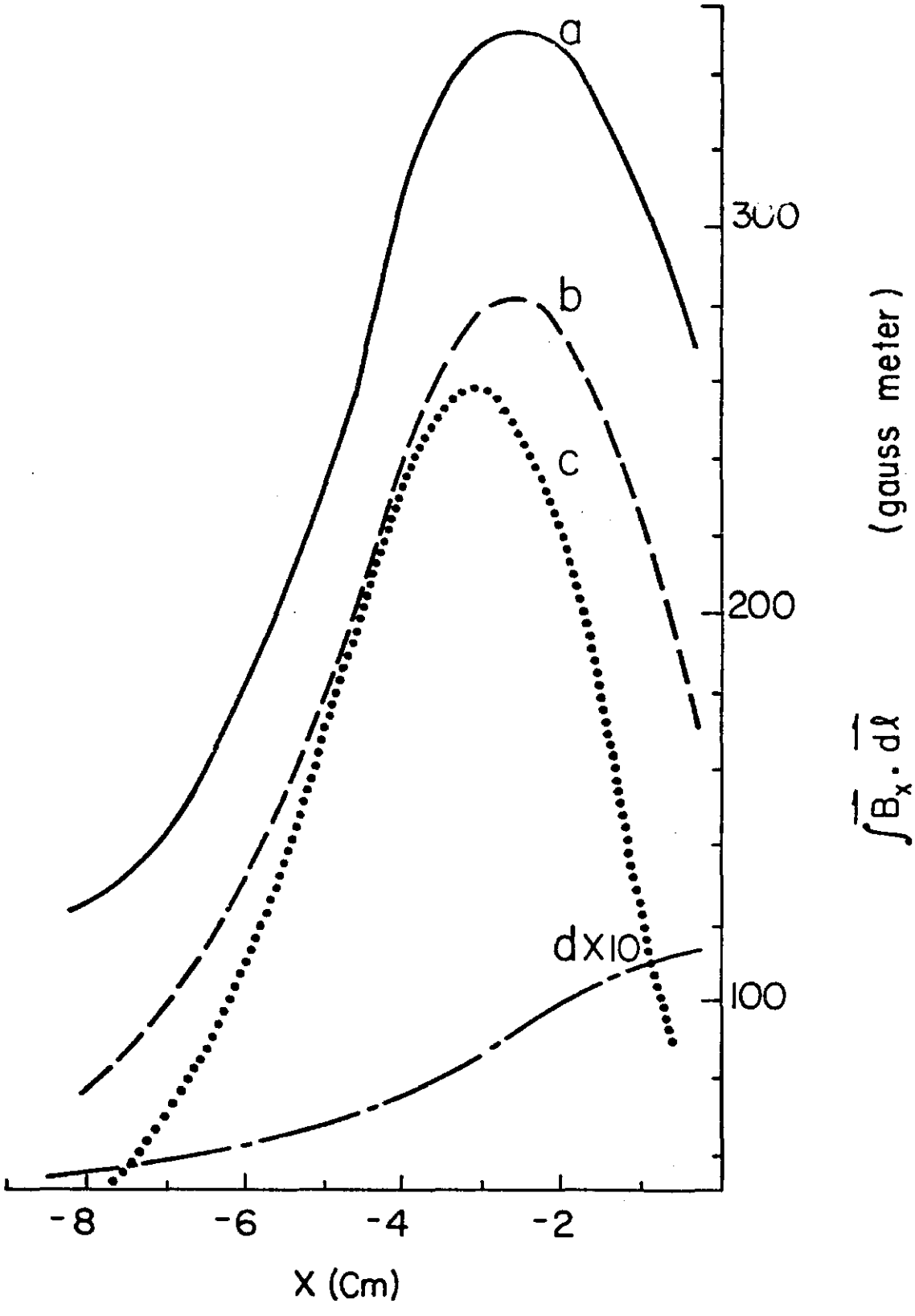
a
b
c
dx10
300
200
100
-8
-6
-4
-2
X (Cm)
$\int \vec{B}_x \cdot d\vec{\ell}$ (gauss meter)

Figure 5

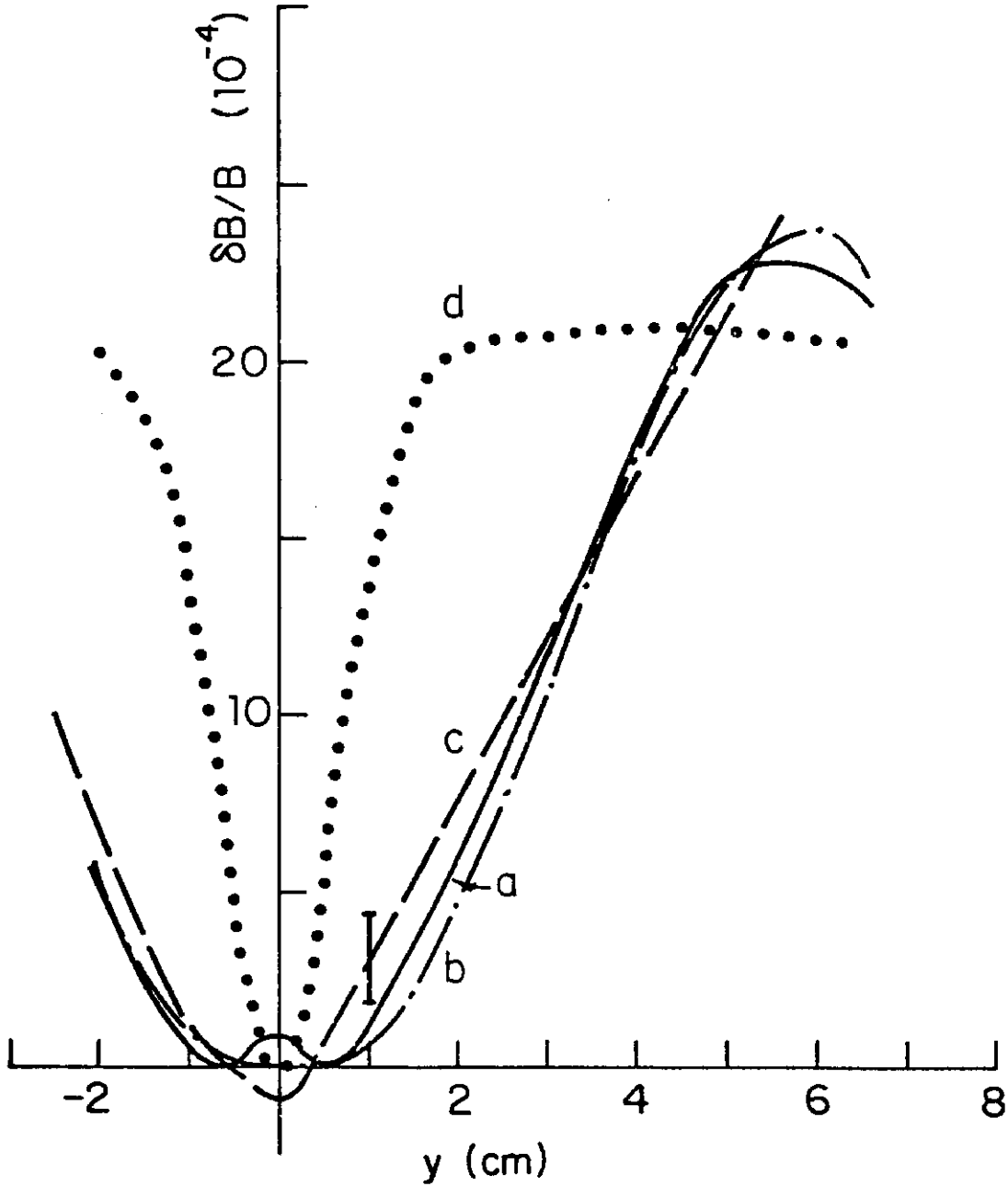

Figure 6

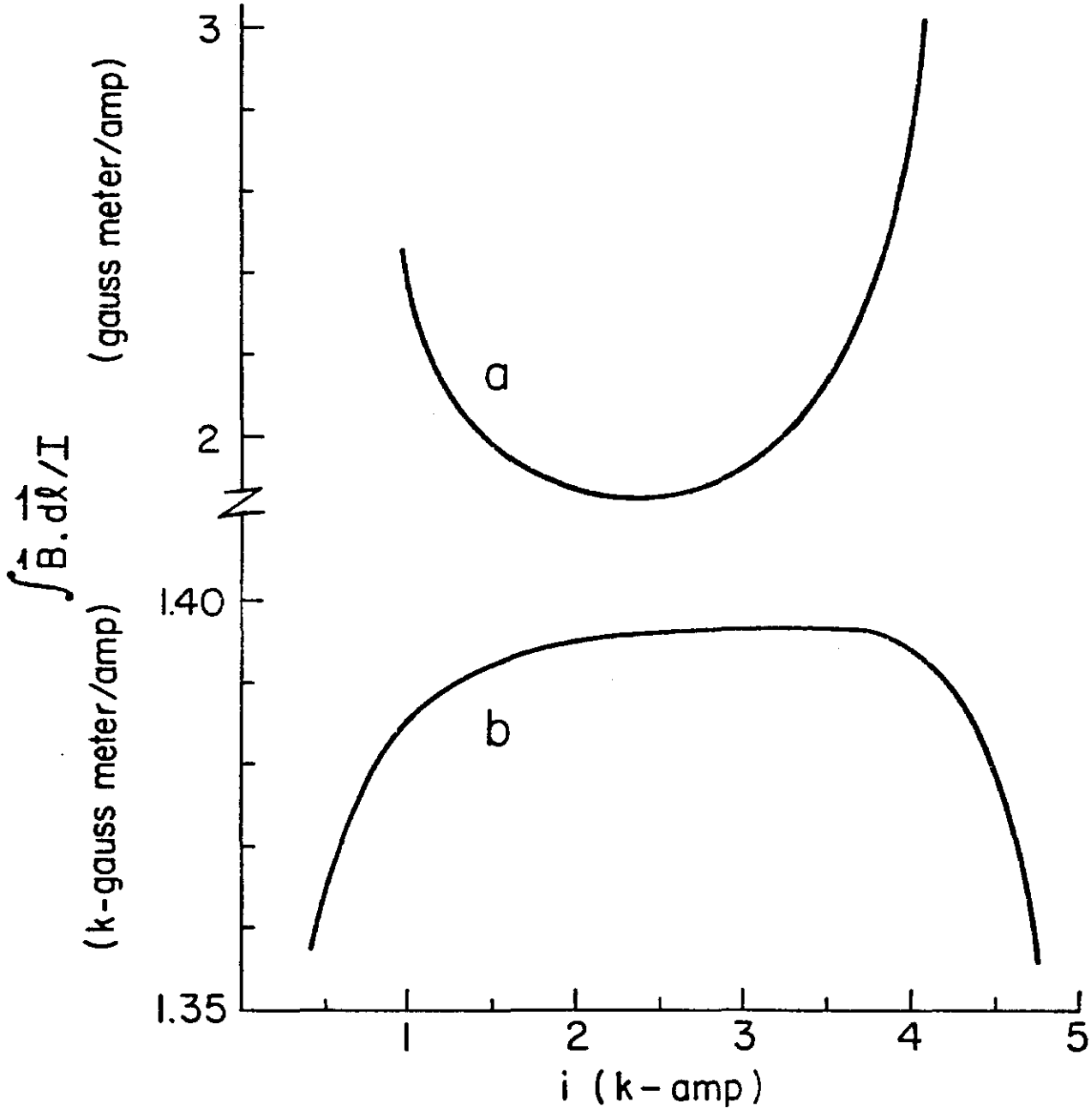
3
2
1.40
1.35
(gauss meter/amp)
(k-gauss meter/amp)
$\int \vec{B} \cdot \frac{d\vec{\ell}}{I}$
a
b
1
2
3
4
5
i (k-amp)

Figure 7

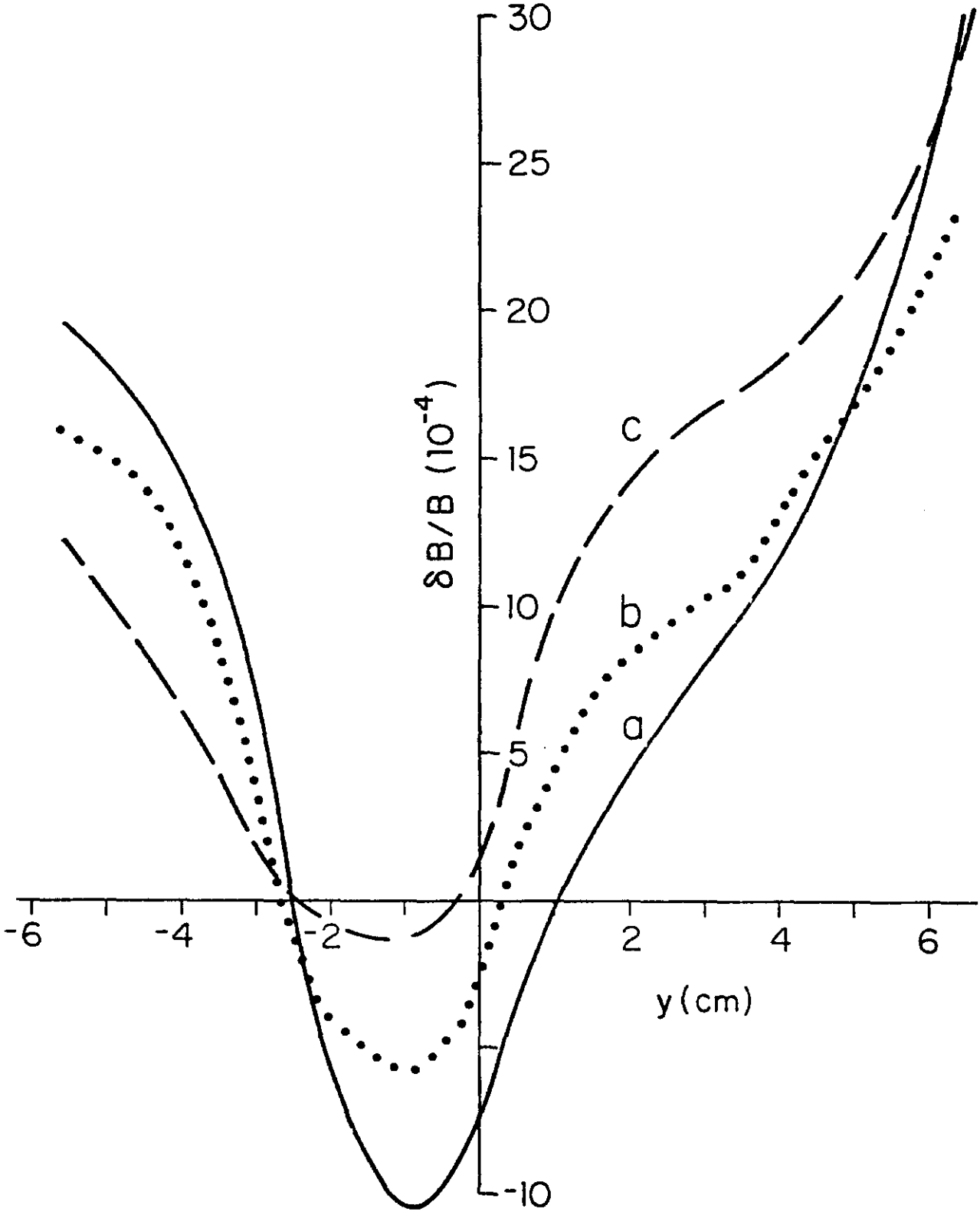

Figure 8

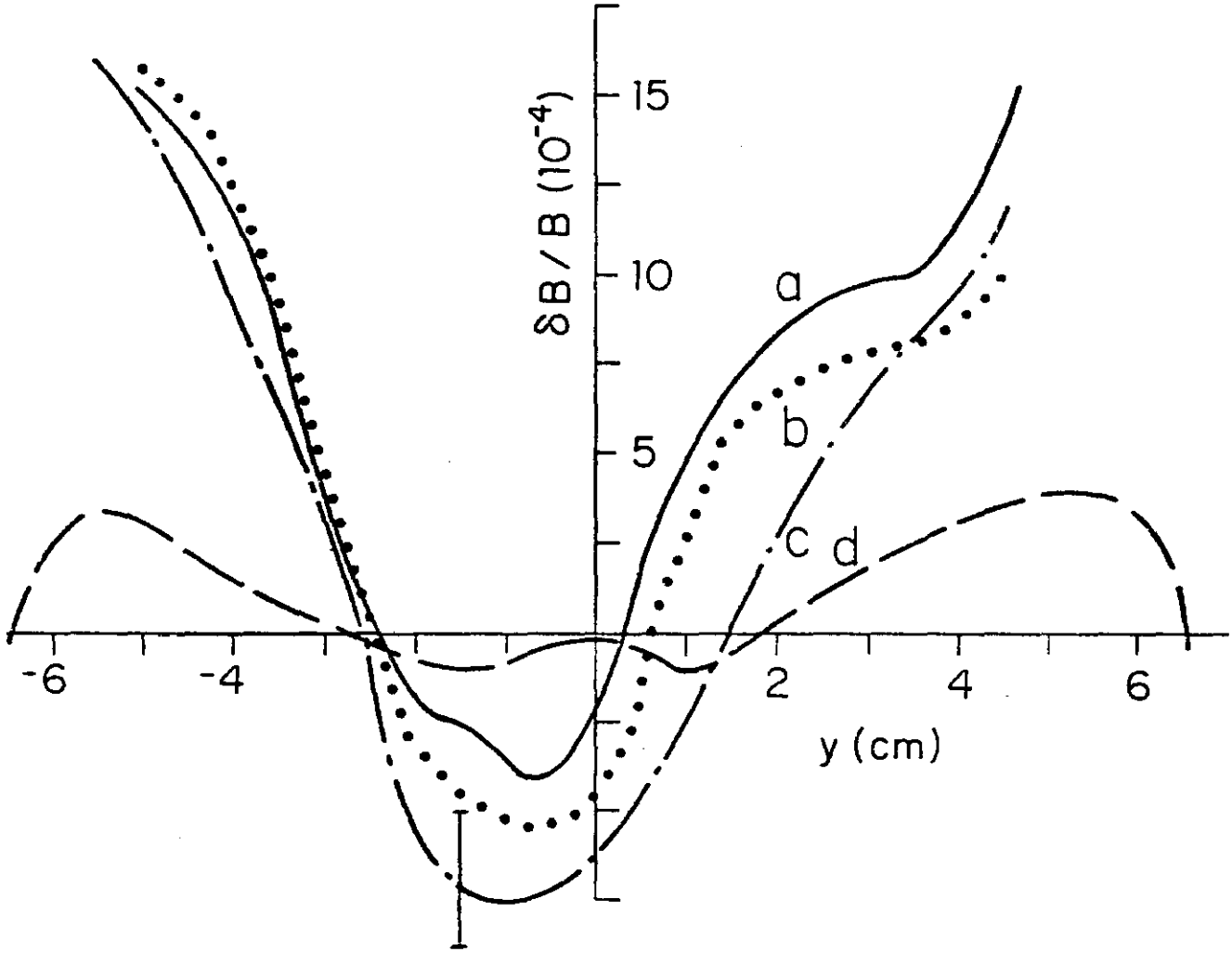

Figure 9

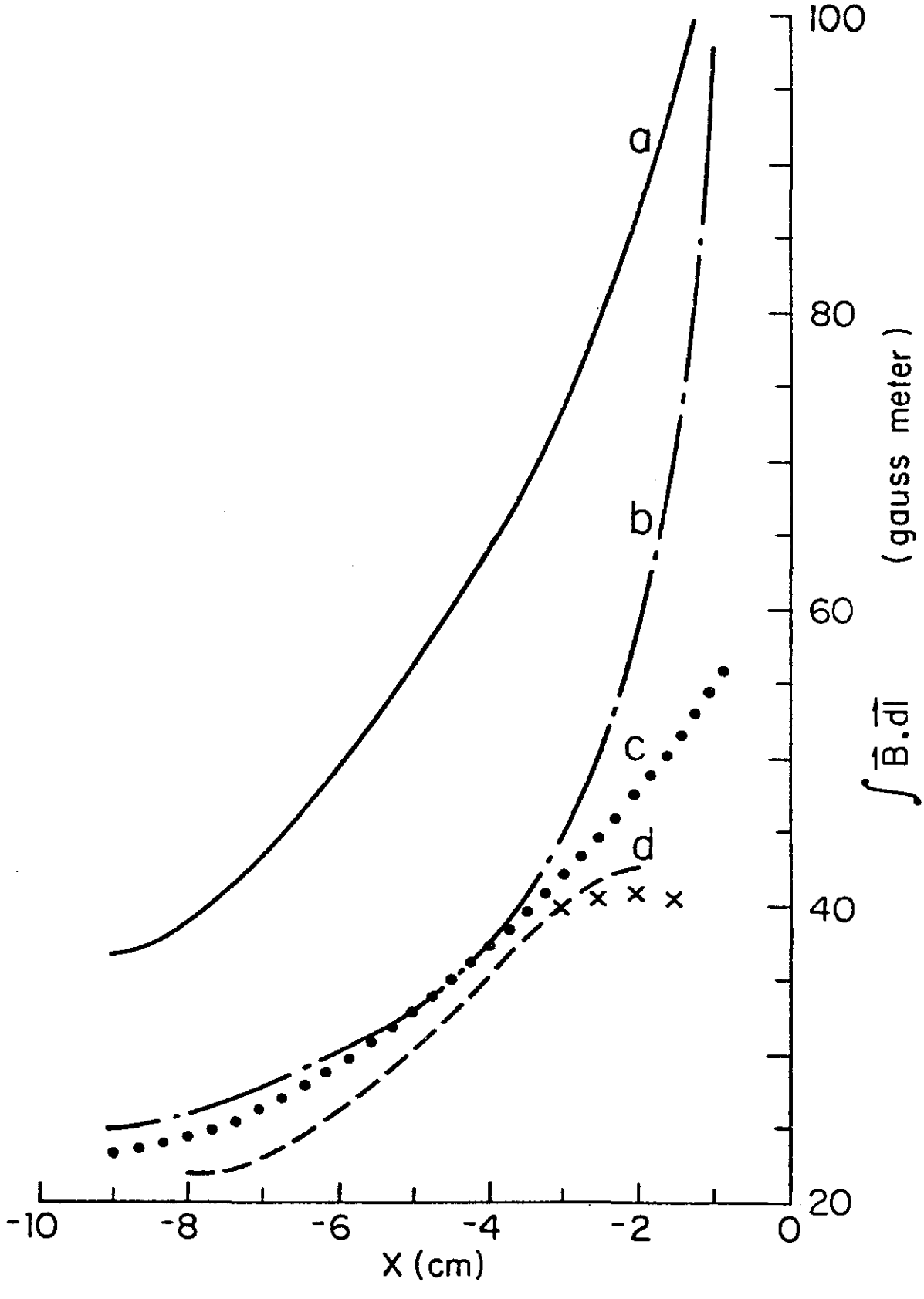

Figure 10

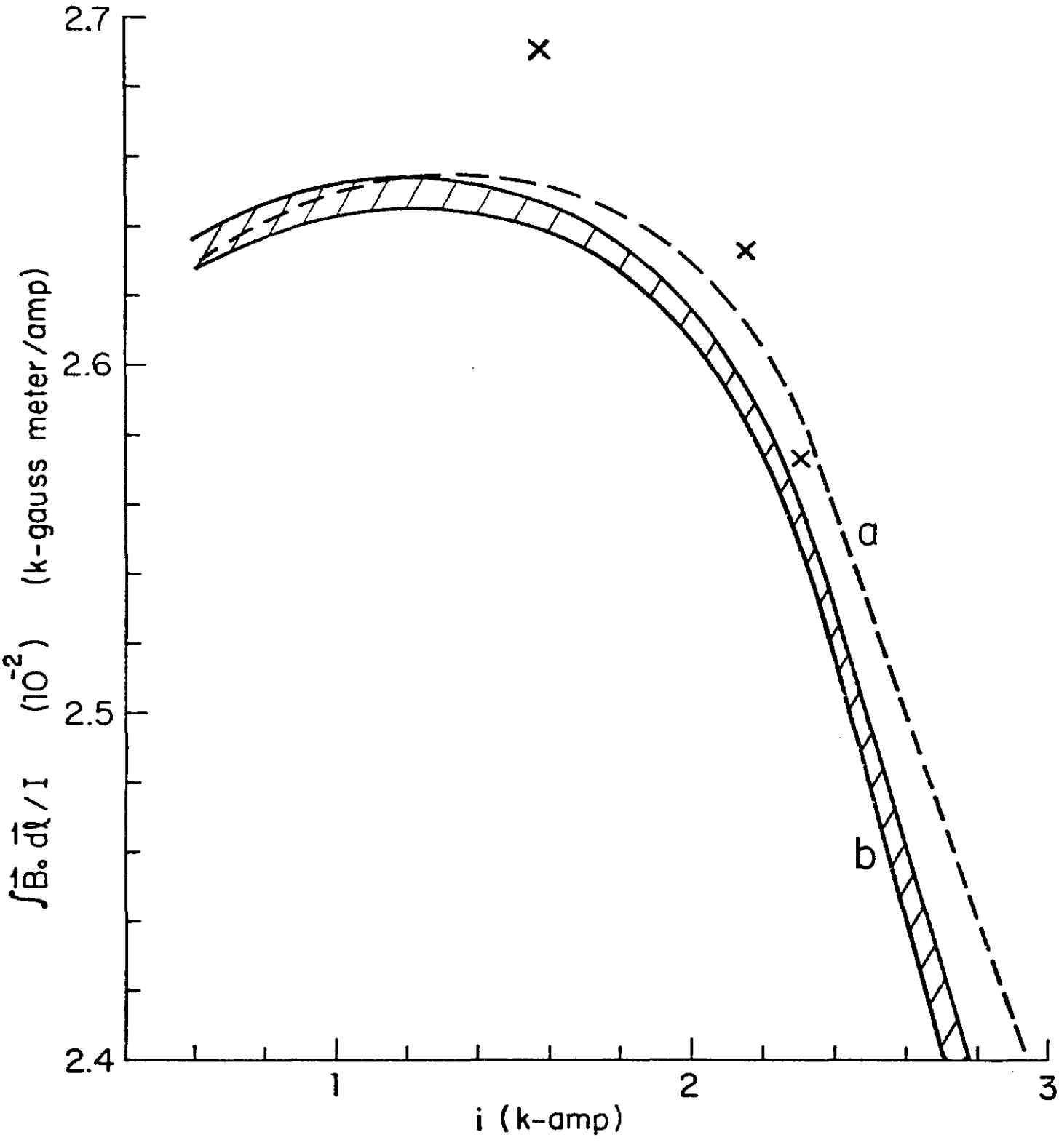
2.7
2.6
2.5
2.4
$\int \frac{1}{B_o} d\ell / I$ (10^{-2}) (k-gauss meter/amp)
1
2
3
i (k-amp)
a
b

Figure 11

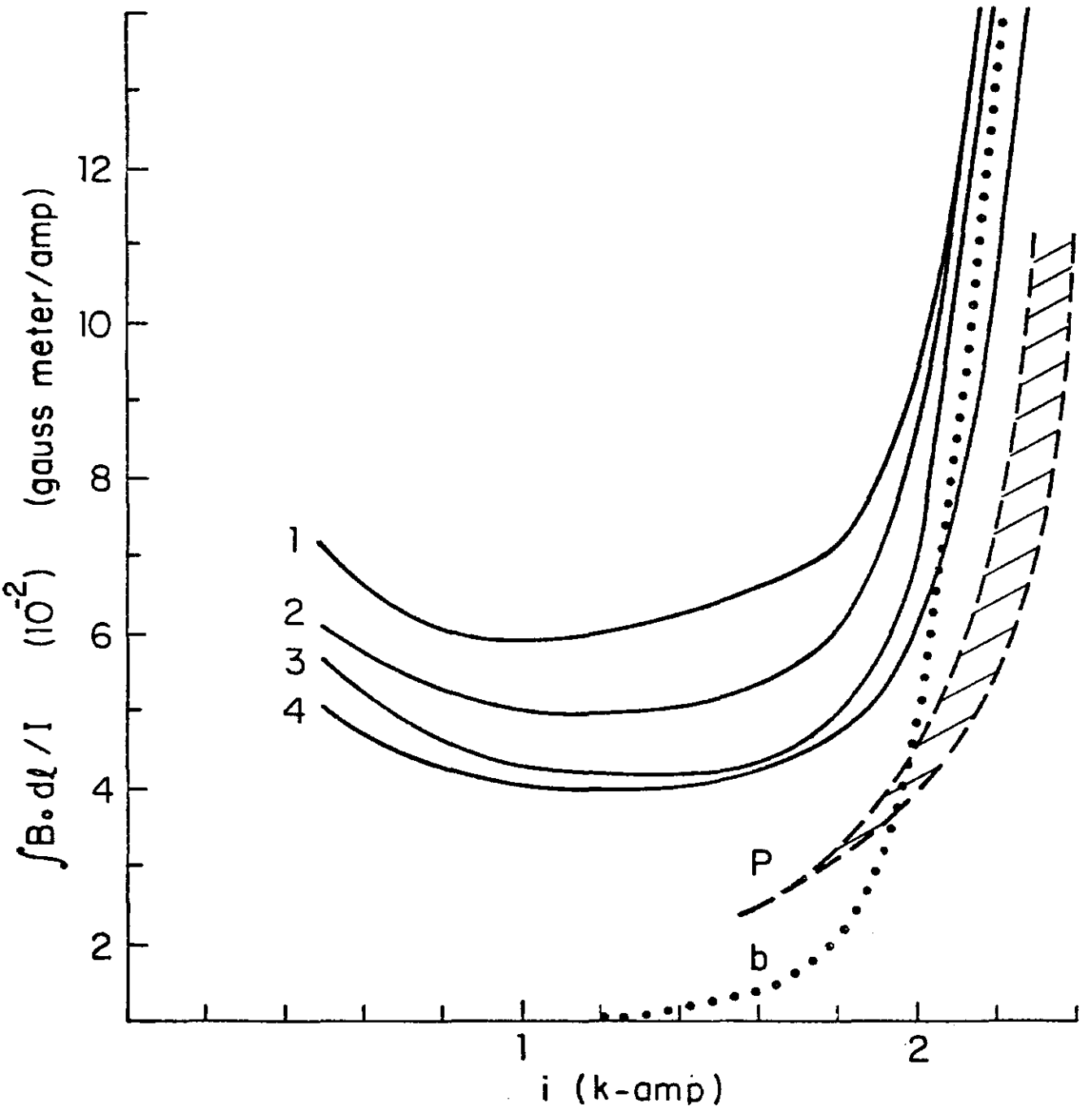
12
10
8
6
4
2
$\int B \cdot d\ell / I$ (10^{-2}) (gauss meter/amp)
1
2
3
4
P
b
1
2
i (k-amp)

Figure 12

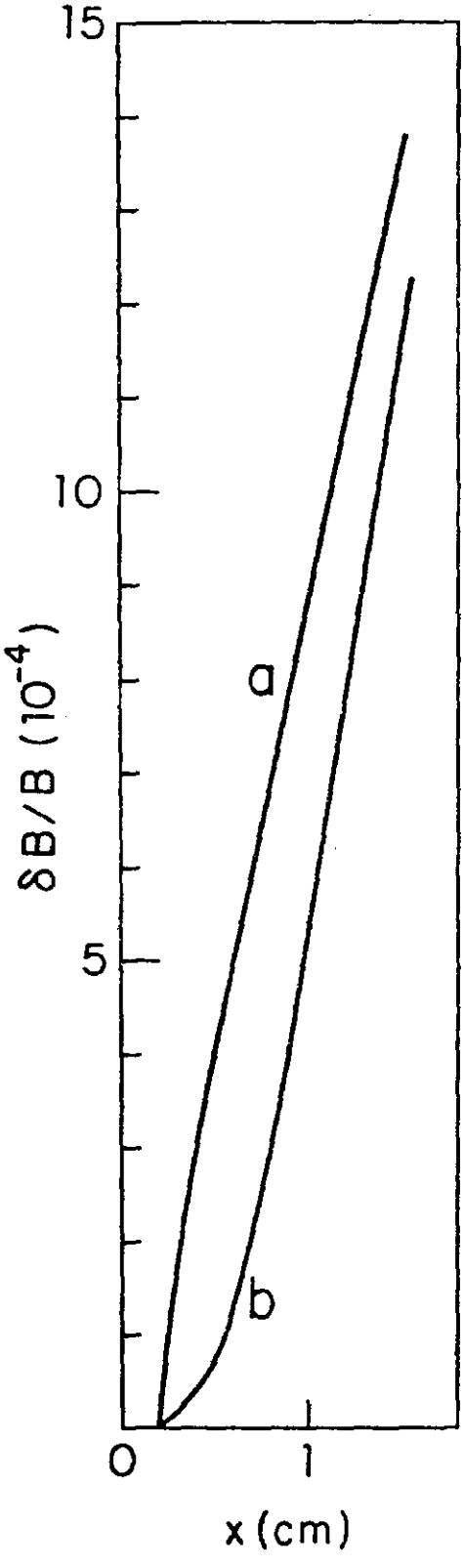

Figure 13

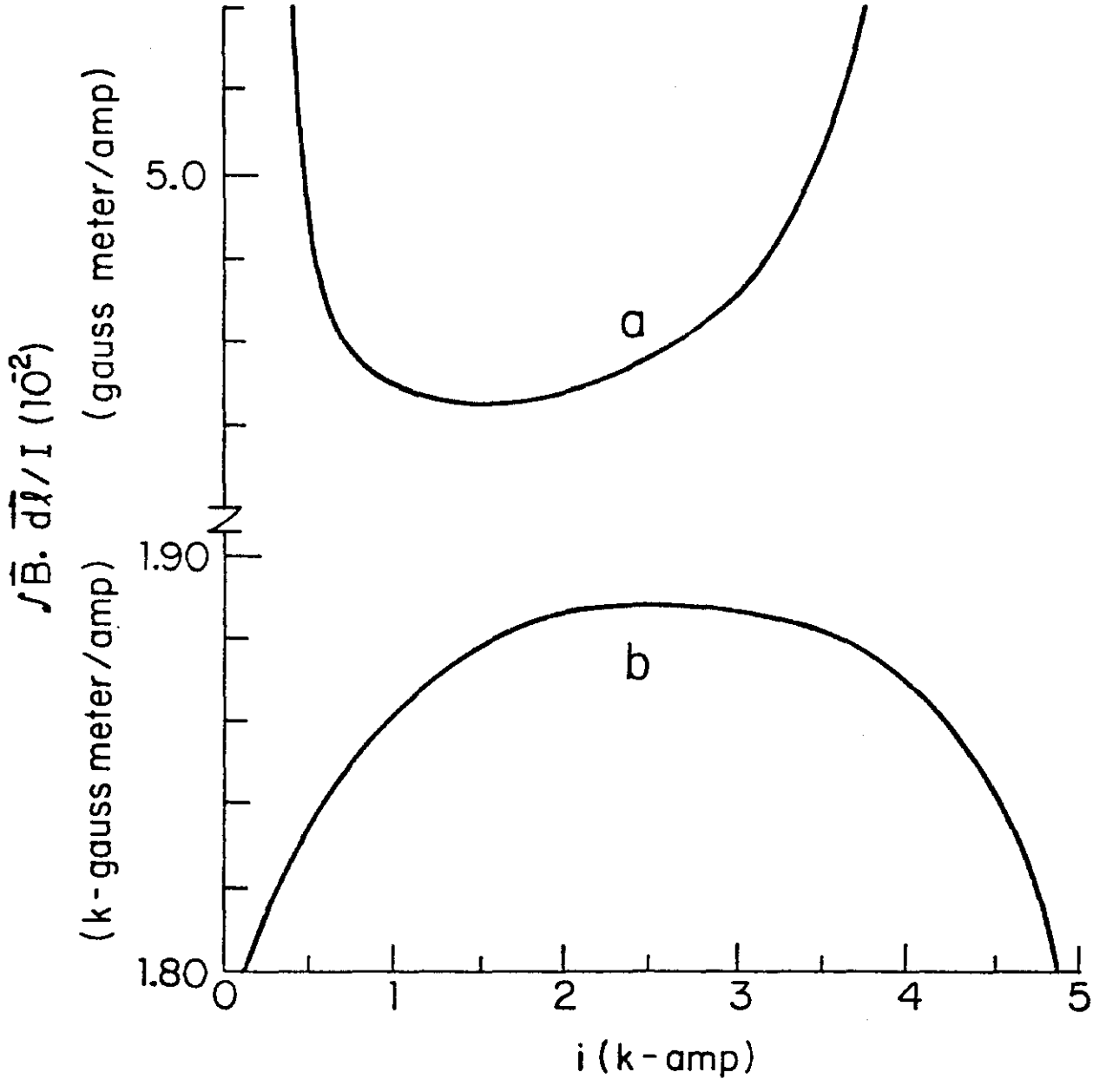

Figure 14

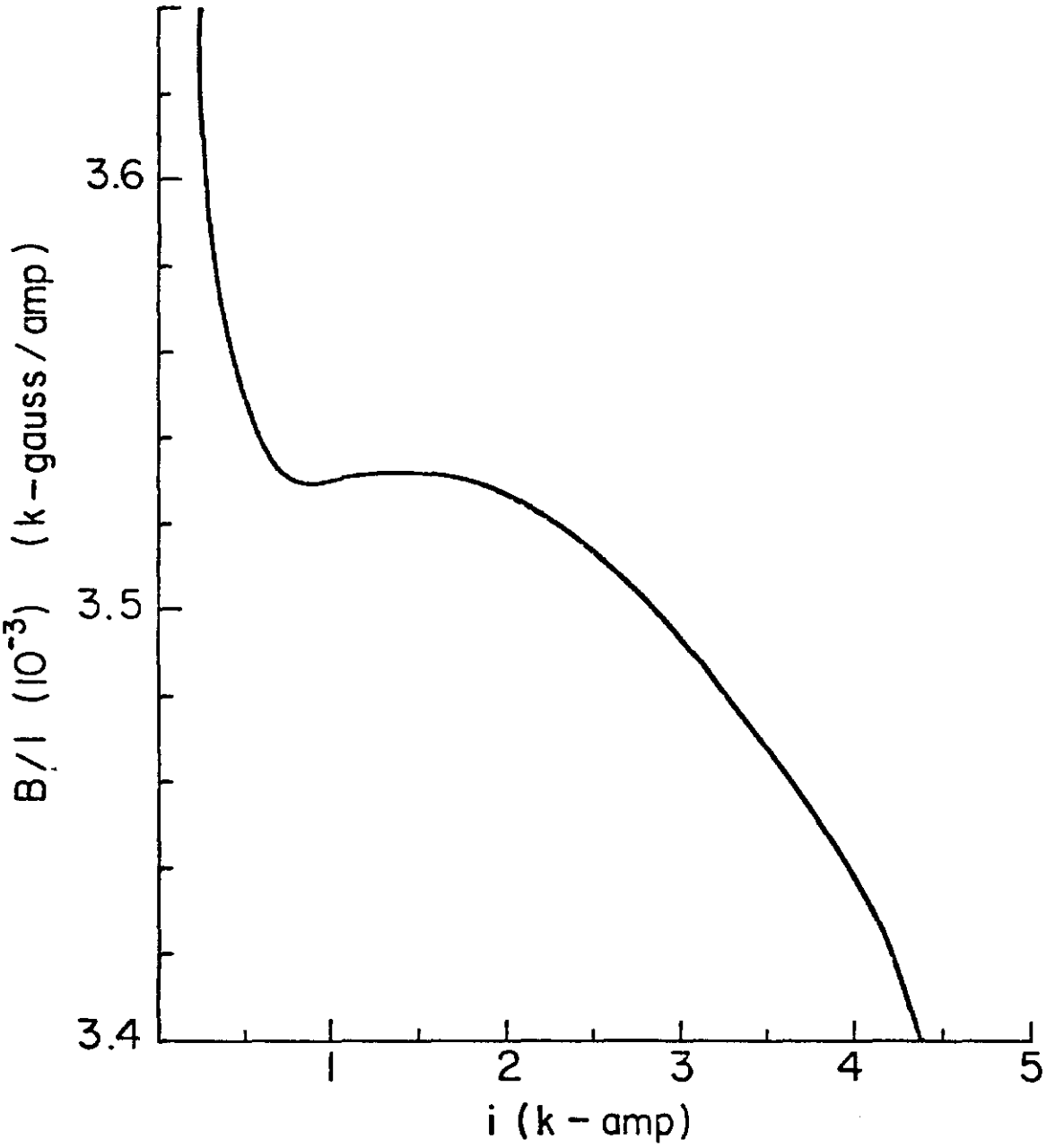

Figure 15

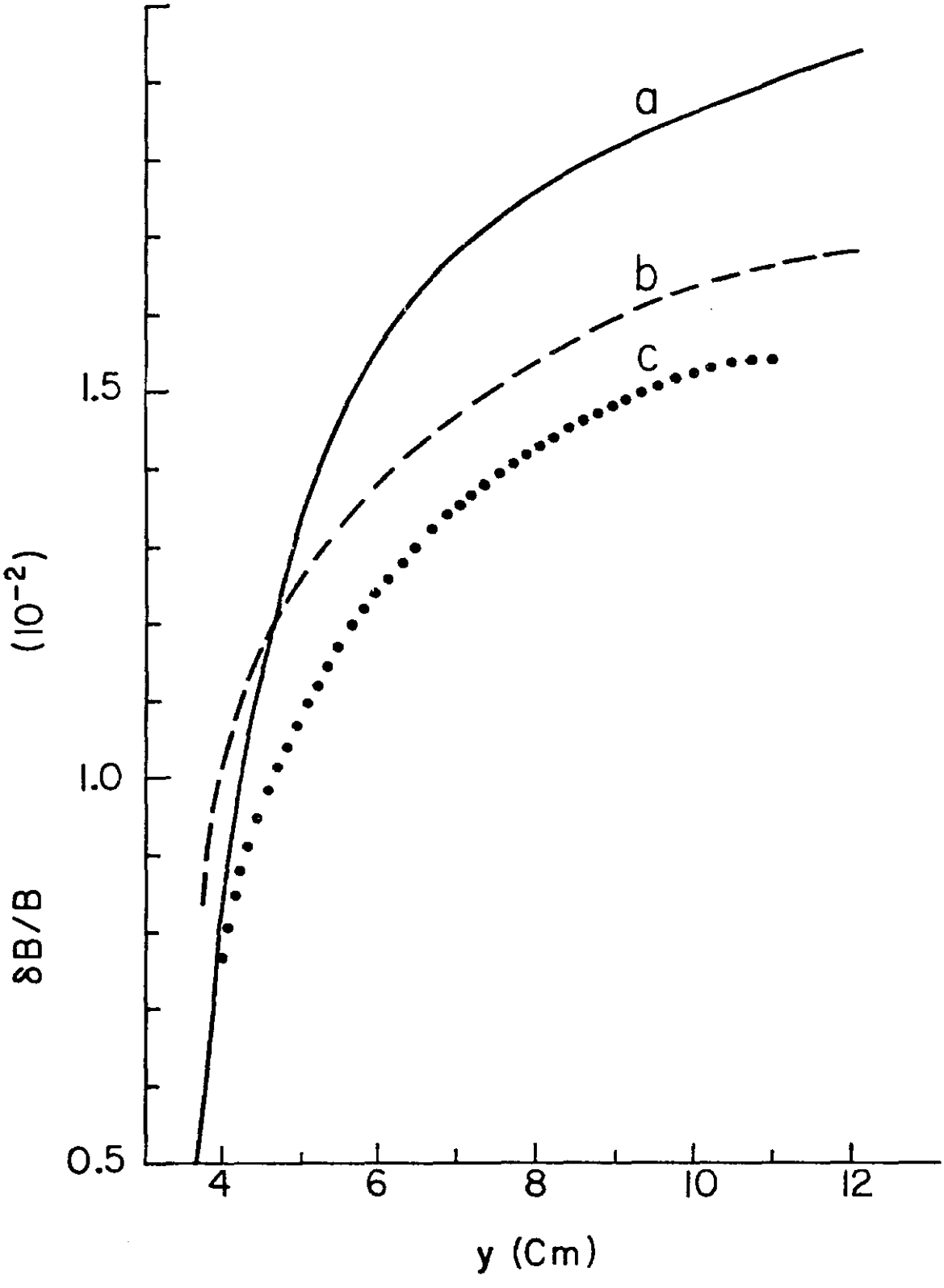

Figure 16

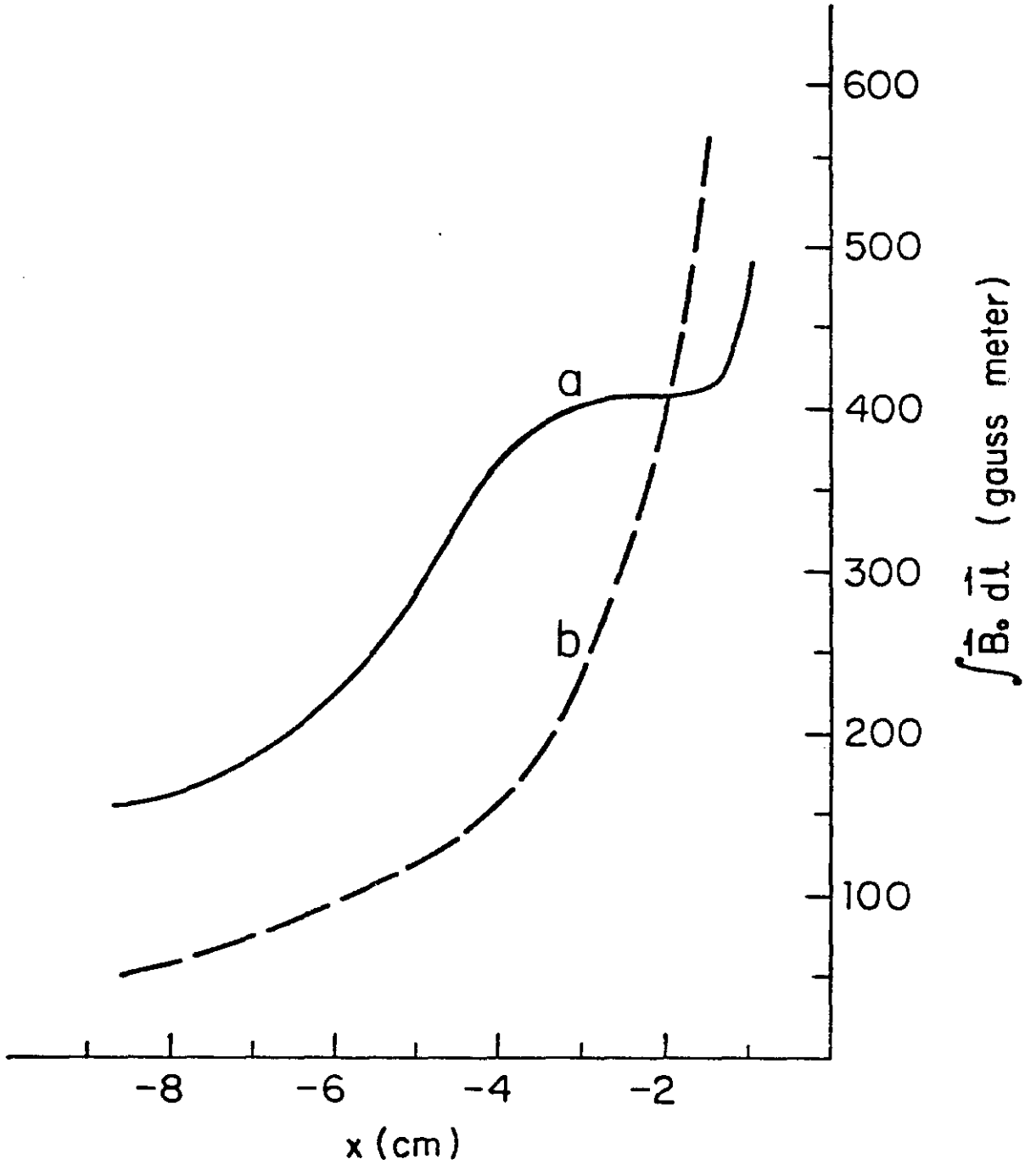

Figure 17

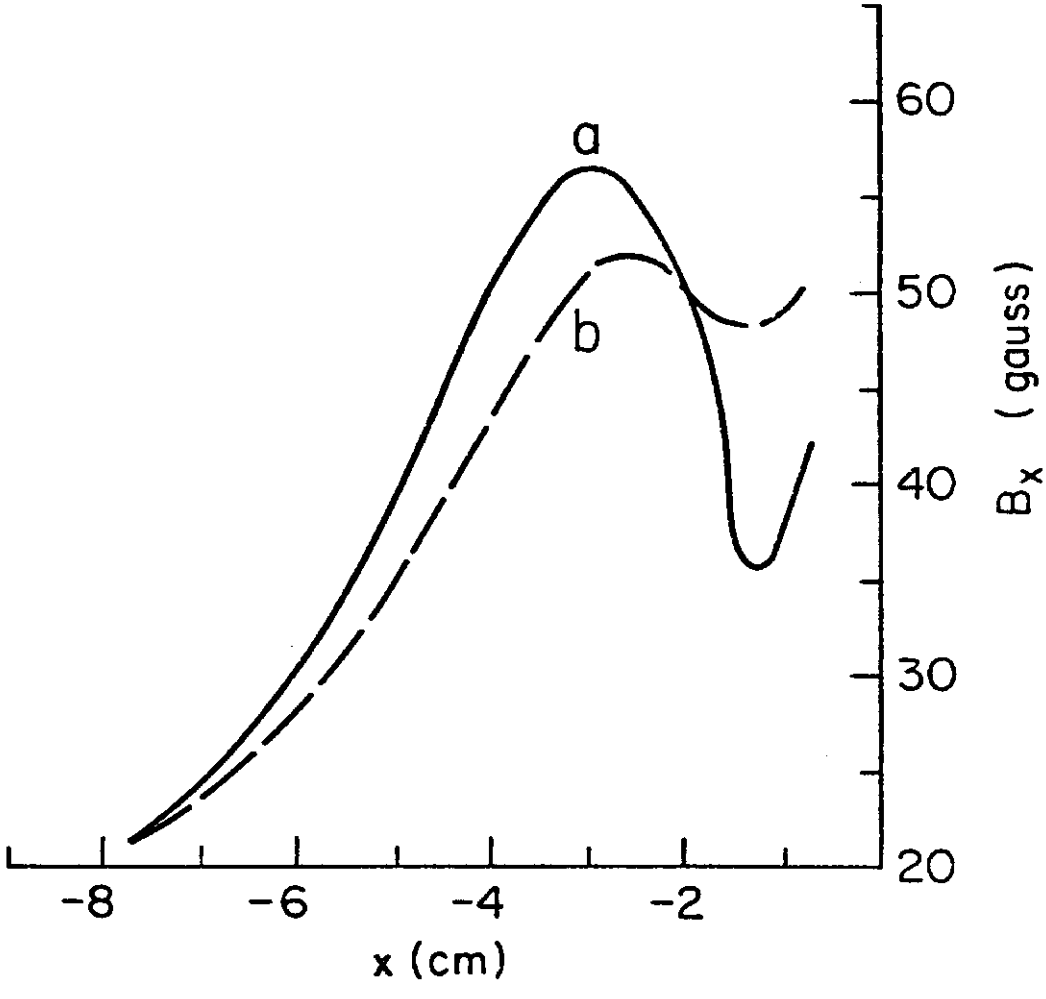

Figure 18

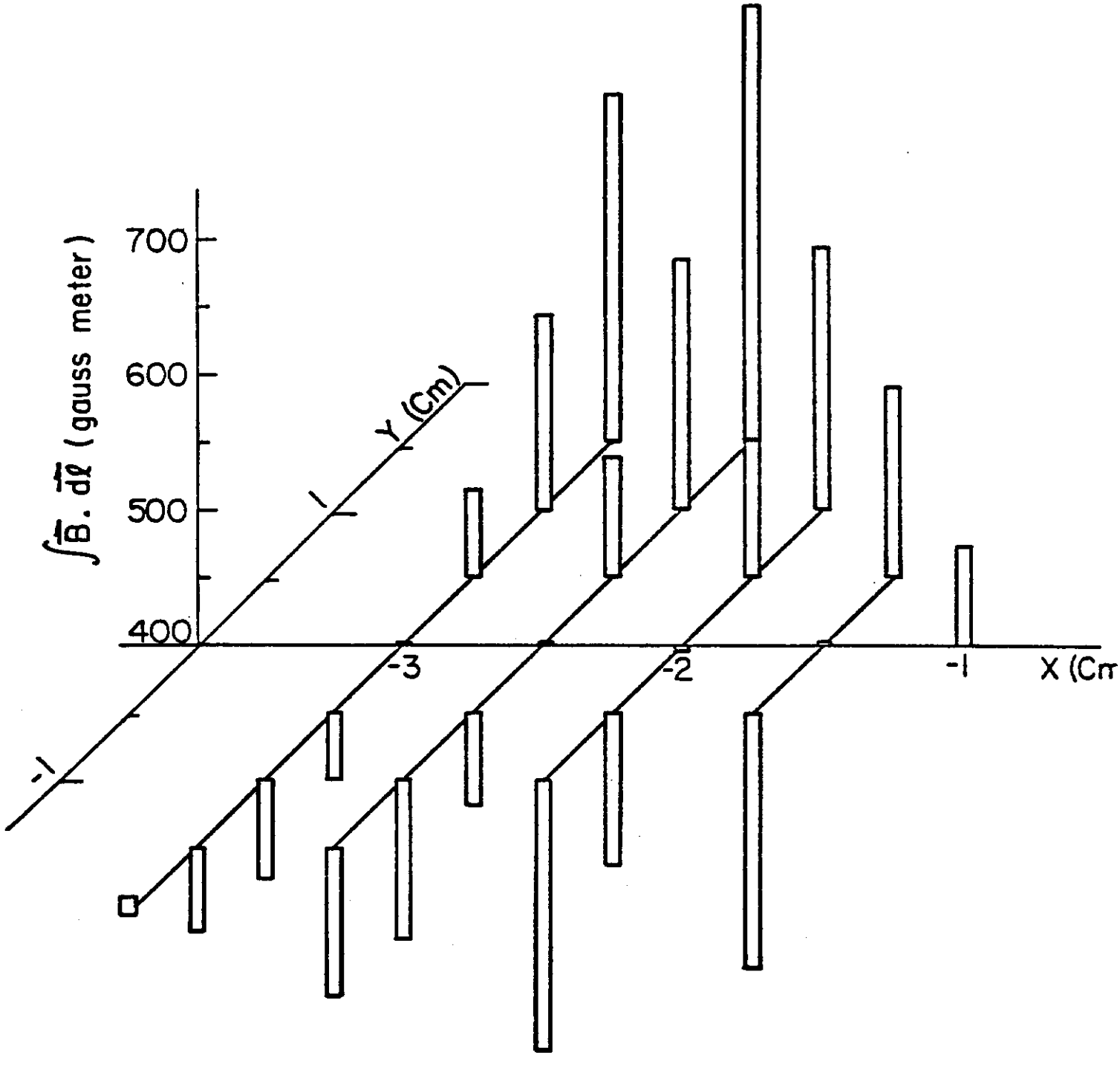
700
600
500
400
$\int \vec{B} \cdot d\vec{\ell}$ (gauss meter)
Y (Cm)
1
-1
-3
-2
-1
X (Cm

Figure 19

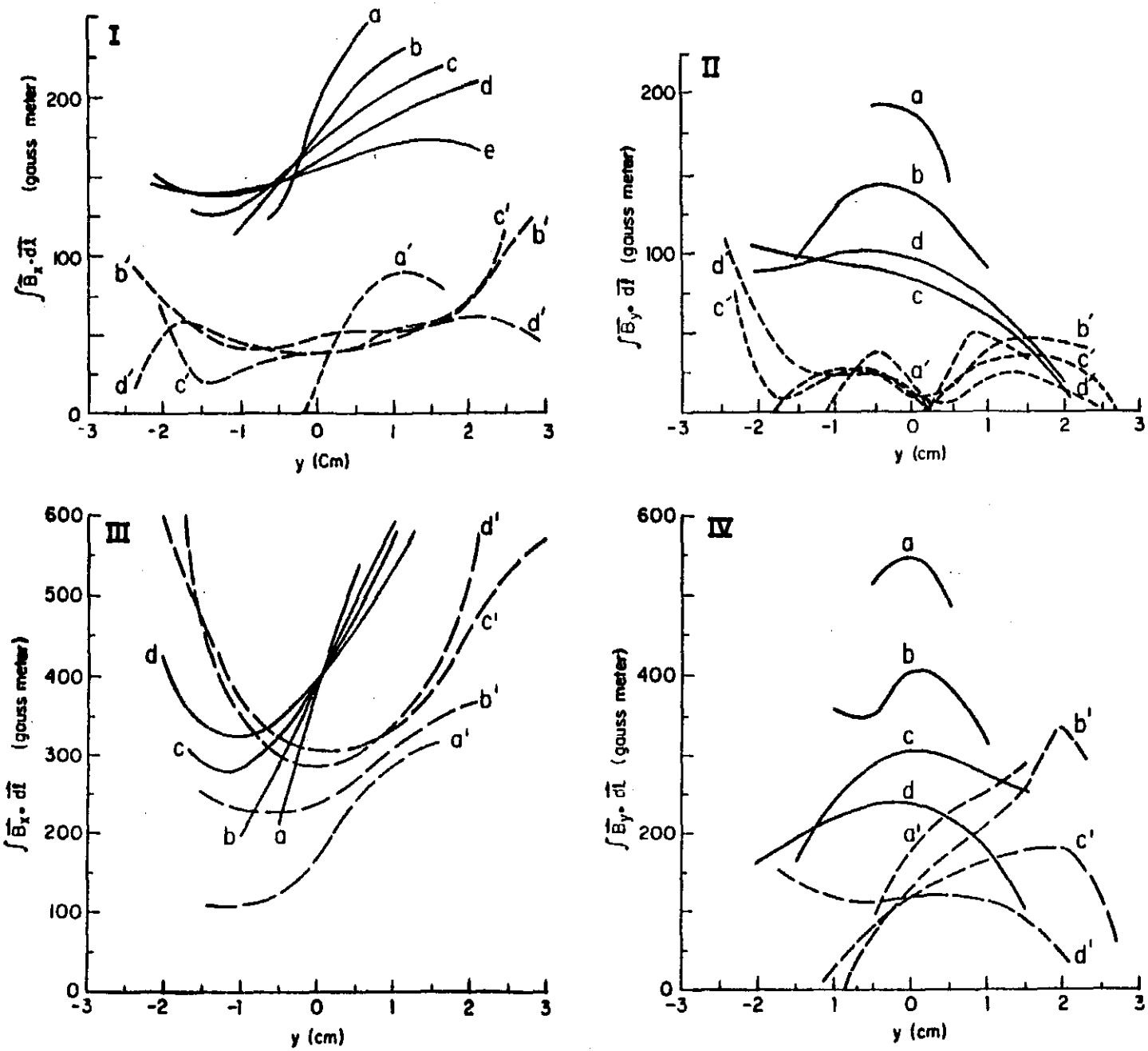

Figure 20